FOI-R--0243--SE
November 2001
ISSN 1650-1942

Scientific report

Åsa Hetyei and Gunilla Efraimsson

A numerical study of acoustic waves in a non-homogeneous flow

Division of Aeronautics, FFA
SE-172 90 STOCKHOLM

FOI-Swedish Defence Research Agency
Division of Aeronautics, FFA
SE-172 90 STOCKHOLM

FOI-R--0243--SE
November 2001
ISSN 1650-1942

Scientific report

Åsa Hetyei and Gunilla Efraimsson

A numerical study of acoustic waves in a non-homogeneous flow

Division of Aeronautics, FFA
SE-172 90 STOCKHOLM

Abstract

A numerical study of acoustic waves propagating in a non homogeneous flow was performed on a two dimensional domain. A subsonic jet flow was used as a base flow to which an acoustic wave was superimposed. It was theoretically and numerically verified that the jet flow model that was used satisfied the Euler equations. In the numerical verification instabilities appeared in the pressure and velocity fields. Since the instabilities were reflected at the outflow boundary and hence would destroy the calculations including acoustic waves, attempts were made to reduce the magnitude of the instabilities before they reached the outflow boundary. Examination of how many grid points that had to be used in order to propagate the acoustic wave in a non-homogenous medium was made.

Table of Contents

1 Introduction

Acoustics in terms of sound is a phenomenon that more or less surrounds everybody in there everyday life and doesn't, most of the time, give rise to any discomfort. Even if the apprehension of sound is very individual, there is no doubt that loud noises such as engine noise can be very disturbing. In the aeronautics industry for example, an important task is to reduce the noise emerging from jet engines.

In a turbo fan engine the rotor blades generate acoustic waves which will give rise to very high sound levels. The generation of sound is a highly non-linear phenomenon, while the propagation is regarded as linear. In order to calculate both the generation and propagation of sound with the same program a non-linear solver has to be utilized. With a second order accurate finite volume solver one has assured the robustness needed in the non-linear parts of the solution. However, the propagation will suffer from damping due to artificial dissipation an dispersive errors unless a very fine mesh is used. In a previous study [1] the propagation of sound waves in a homogenous media was studied. In this report we evaluate a second order finite volume solver when computing the sound field of acoustic waves propagating in air with non constant speed of sound. Also, different outflow boundary conditions are examined.

In this study we solve the Euler equations on a two dimensional domain. As a base flow a subsonic jet flow is considered. An acoustic wave is superimposed onto the jet flow at the inflow boundary. A cell centered finite volume method is used to discretize the Euler equations in space. An implicit time marching with explicit subiterations was used for the integration in time.

This thesis contain results from several tests with different boundary conditions, grid sizes and parameters such as cuff-off ratio, disturbance amplitude and points per wave length.

2 The Euler Equations

2.1 Jet flow

In this report we calculate a flow field containing acoustic waves which propagate in air with non constant speed of sound. As a profile of the non constant base flow, a two dimensional y-periodic jet flow was considered.

In this study we consider the Euler equations in two dimensions

$$\frac{\partial U}{\partial t} + \vec{\nabla} \cdot \vec{F} = 0 \tag{2-1}$$

The vector U of conservative variables is

$$U = \begin{bmatrix} \rho \\ \rho \vec{v} \\ \rho E \end{bmatrix} = \begin{bmatrix} \rho \\ \rho u \\ \rho v \\ \rho E \end{bmatrix} \tag{2-2}$$

where ρ is the density, u is the velocity in the x-direction, v is the velocity in the y-direction and E is the total energy.

The flux vector $\vec{F}$ can be written as

$$\vec{F} = \begin{bmatrix} \rho \vec{v} \\ \rho \vec{v} \otimes \vec{v} + p\bar{I} \\ \rho \vec{v} H \end{bmatrix} \tag{2-3}$$

Here is p the pressure and $\bar{I}$ represents the 2×2 unit matrix. The total enthalpy H is defined as $H = E + \frac{p}{\rho}$. The tensor product $\otimes$ gives the matrix $v_i v_j$, where v_i is a component of the velocity vector.

Here we consider calorically perfect gases, with the equation of state

$$p = (\gamma - 1)\left(\rho E - \frac{1}{2}\rho(u^2 + v^2)\right) \tag{2-4}$$

In this report all body forces are neglected.

We solved the Euler equations, Eqn. (2-1), on a 2D-rectangle, with height $H = 0.2$ and length $L = 0.2$, see Fig. 2-1.

Fig. 2-1. Computational domain.

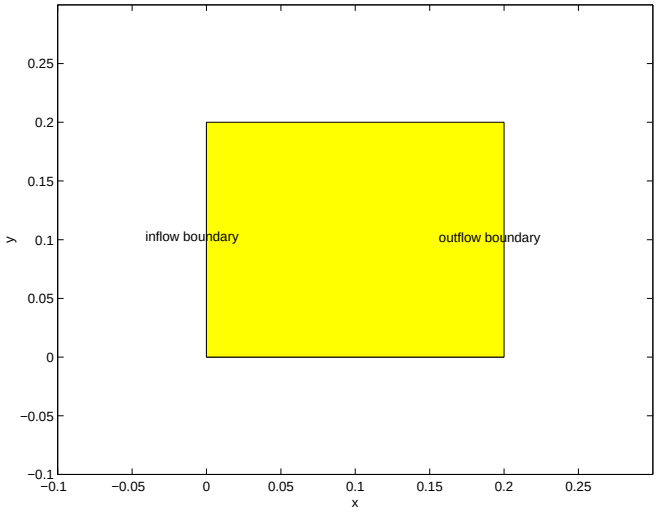

The inflow boundary is at $x = 0$ and the outflow boundary at $x = 0.2$. The problem is periodic in the y-direction.

As a base flow we consider a subsonic laminar jet flow. The jet is modelled as in [2]. That is the velocity in the x-direction and the temperature are specified as

$$u(y) = \frac{1}{2}[(u_c + u_\infty) + (u_c - u_\infty)\tanh(a(y - y_1))] \tag{2-5}$$

$$T(y) = T_\infty + (T_c - T_\infty)(u/u_c - u_\infty/u_c)/(1 - u_\infty/u_c) \tag{2-6}$$

$$+0.5(\gamma - 1)M^2(1 - u/u_c)(u/u_c - u_\infty/u_c)$$

See Fig. 2-2.

The parameter a in (2-5) determines the sharpness of the velocity profile. u_∞ and T_∞ are free stream values, u_c and T_c are values at $y = 0.5H$, respectively. M is the Mach number at $y = 0.5H$.

The pressure is specified as

$$p(0, y) = constant \tag{2-7}$$

Also, the velocity in the y-direction is set to zero, i.e.

$$v = 0 \tag{2-8}$$

The density of the jet can now be calculated by using the ideal gas law, $\rho_{jet} = (p_{jet})/(R_{gas} \cdot T_{jet})$.

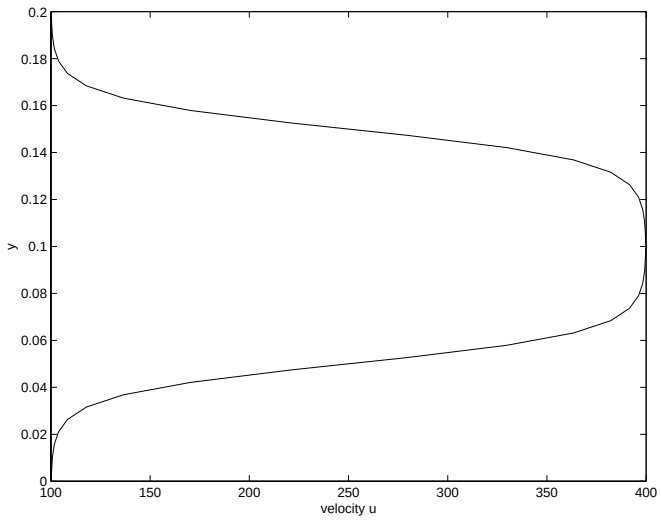

Fig. 2-2. Velocity in the x-direction, u, of the jet.

We also check that the flow field described by (2-5) through (2-8) is a steady state solution of the Euler equations, Eqn (2-1). Consider the Euler equations on the form

$$\frac{\partial \rho}{\partial t} + \frac{\partial}{\partial x}(\rho u) + \frac{\partial}{\partial y}(\rho v) = 0 \tag{2-9}$$

$$\begin{aligned} &\frac{\partial}{\partial t}(\rho u) + \frac{\partial}{\partial x}(\rho u^2) + \frac{\partial}{\partial y}(\rho uv) + \frac{\partial p}{\partial x} = 0 \\ &\frac{\partial}{\partial t}(\rho v) + \frac{\partial}{\partial x}(\rho uv) + \frac{\partial}{\partial y}(\rho v^2) + \frac{\partial p}{\partial y} = 0 \end{aligned} \tag{2-10}$$

$$\begin{aligned} &\frac{\partial}{\partial t}\left[\rho\left(e + \frac{u^2+v^2}{2}\right)\right] + \frac{\partial}{\partial x}\left(\rho\left(e + \frac{u^2+v^2}{2}\right)u\right) + \frac{\partial}{\partial y}\left(\rho\left(e + \frac{u^2+v^2}{2}\right)v\right) \\ &+ \frac{\partial}{\partial x}(pu) + \frac{\partial}{\partial y}(pv) = 0 \end{aligned} \tag{2-11}$$

where $e = c_V T$. c_V is the specific heat capacity at constant volume defined as $c_V = \left(\frac{\partial e}{\partial T}\right)_V$.

The jet flow described by (2-5)-(2-8) is a 2-D time independent problem. Also we have that $v = 0$, $\frac{\partial v}{\partial y} = 0$, $\frac{\partial p}{\partial y} = 0$ and $\frac{\partial p}{\partial x} = 0$ yielding that the Euler equations are simplified to

$$\begin{aligned} &\frac{\partial}{\partial x}(\rho u) = 0 \\ &\frac{\partial}{\partial x}(\rho u^2) = 0 \\ &\frac{\partial}{\partial x}(\rho c_v T u) + \frac{\partial}{\partial x}\left(\frac{\rho u^3}{2}\right) + \frac{\partial}{\partial x}(pu) = 0 \end{aligned} \tag{2-12}$$

or equivalently

$$\begin{aligned} \rho u &= f_1(y) \\ \rho u^2 &= f_2(y) \\ \rho c_v T u + \frac{\rho u^3}{2} + p u &= f_3(y) \end{aligned} \tag{2-13}$$

In our model of the jet flow we assume that $u = g_1(y)$, $T = g_2(y)$ and $\rho = g_3(T(y))$, and hence (2-5)-(2-8) is a solution to the Euler equations.

2.2 Wave input

At the inflow boundary we also give an acoustic wave as inflow data. We let

$$\begin{aligned} p &= p_{jet} + p' \\ u &= u_{jet} + u' \\ v &= v_{jet} + v' \\ \rho &\text{ given by isentropic flow} \end{aligned} \tag{2-14}$$

where

$$\begin{aligned} p'(0,y) &= p_0 \sin\left(\omega t + 2\pi \frac{y}{H}\right) \\ u'(0,y) &= \left(\frac{1}{\omega/(k_x c) - \bar{M}(y)}\right) \frac{p'}{\bar{\rho}(y) c} \\ v'(0,y) &= \frac{k_y}{k_x} u \end{aligned} \tag{2-15}$$

In (2-15) $\bar{M}(y)$ and $\bar{\rho}$ is the Mach number and the density in the jet. For down-stream travelling waves the wave numbers in x- and y- direction, k_x and k_y, can be defined in terms of the so called cut-off ratio ξ as

$$\frac{k_x}{k_y} = \frac{-\bar{M}(y)\xi + \sqrt{\xi^2 - 1}}{\sqrt{1 - \bar{M}(y)^2}} \tag{2-16}$$

The ratio $\omega / k_x c$ can be calculated from the above ratio using the definition of the cut-off ratio as

$$\omega / k_x c = \frac{\xi \sqrt{1 - \bar{M}(y)^2}}{k_x / k_y} \tag{2-17}$$

The definition of the cut-off ratio is

$$\xi = \frac{\omega}{ck_y\sqrt{1-\overline{M}(y)^2}} \quad \text{where} \quad k_y = \frac{2\pi}{N_\theta \Delta y} \tag{2-18}$$

$\xi > 1$ means that the wave will propagate, while $\xi < 1$ means that the wave will evanesce.

3 Numerical method

All computations in this report were performed with the structured finite volume Navier-Stokes solver Euranus [3]. In this section we briefly describe the features used in this report.

3.1 Cell centered finite volume method

The discretization in space is a second order accurate cell centred finite volume method. That is equation (2-1) is discretized as

$$\int_{\Omega} \frac{\partial U}{\partial t} d\Omega + \sum_{faces} (\vec{F_I} \cdot \vec{n})^* \Delta S = 0 \tag{3-1}$$

where $\vec{F_I} \cdot \vec{n}$ are the inviscid flux. The sum of the flux terms refers to all the external sides of a control volume Ω. For cell $1(i, j)$ in figure (3-1), Ω is the area ABCD, and the flux terms will be summed over the four sides AB, BC, CD, DA. We also have $\vec{n}$ which is the unit normal vector of the cell surface considered and ΔS which is the cell surface area. The solution is obtained in the cell centres.

Fig. 3-1. 2D cell centered structured finite volume mesh.

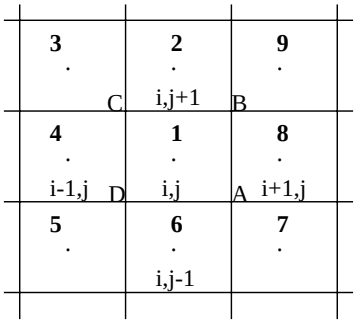

The inviscid numerical flux is expressed as

$$(\vec{F_I} \cdot \vec{n})^*_{i+1/2} = \frac{1}{2}\{(\vec{F} \cdot \vec{n})_i + (\vec{F} \cdot \vec{n})_{i+1}\} - d_{i+1/2} \tag{3-2}$$

The first term on the right-hand-side corresponds to a purely central evaluation of the flux. The term $d_{i+1/2}$ represents a numerical dissipation term, that may be an numerical dissipation used in combination with central schemes, or the dissipation associated with upwind schemes. In this report we only use a central scheme.

For the central scheme, we used a Jameson type dissipation with 2nd and 4th order derivatives of the conservative variables

$$d_{i+1/2} = \varepsilon^{(2)}{}_{i+1/2}\delta U_{i+1/2} + \varepsilon^{(4)}{}_{i}\delta^2 U_i - \varepsilon^{(4)}{}_{i+1}\delta^2 U_{i+1} \tag{3-3}$$

where the difference operators are defined as,

$$\delta = E^{1/2} - E^{-1/2} \tag{3-4}$$

$$\delta^2 = (\delta)^2 = E^1 - 2E^0 + E^{-1} \tag{3-5}$$

Here the displacement operator E is defined as

$$E^j U_i = U_{i+j} \tag{3-6}$$

The scalar coefficients ε in (3-3) are given by

$$\varepsilon^{(2)}{}_{i+1/2} = \frac{1}{2}\kappa^{(2)}\lambda^* max(v_{i-1}, v_i, v_{i+1}, v_{i+2}) \tag{3-7}$$

$$\varepsilon^{(4)}{}_{i+1/2} = max\left(0, \frac{1}{2}\kappa^{(4)}\lambda^* - \varepsilon^{(2)}{}_{i+1/2}\right)$$

The coefficients $\kappa^{(2)}$, $\kappa^{(4)}$ are user input, chosen as small as possible to stabilize the numerical scheme while having the least impact on the solution.

The cell centred values of $\varepsilon^{(4)}{}_i$ in equation (3-3) are obtained by arithmetic averaging of the cell face values of equation (3-7). The variables v_i are sensors to activate the second-difference dissipation in regions of strong gradients, such as shocks, and to de-activate it elsewhere. They measure variations of pressure and are defined as

$$v_i = \left|\frac{p_{i+1} - 2p_i + p_{i-1}}{p_{i+1} + 2p_i + p_{i-1}}\right| \tag{3-8}$$

λ^* in (3-7) is a measure of the characteristic speeds and is commonly chosen as the spectral radius multiplied with the cell face area

$$\lambda^* = \lambda^*{}_{i+1/2} = (\vec{v} \cdot \overrightarrow{\Delta S} + c\Delta S)_{i+1/2} \tag{3-9}$$

The surface area, ΔS, and the normal to the surface, $\overrightarrow{\Delta S} = \Delta S\vec{n}$, are defined from the interface surface in question for the flux evaluation.

3.2 Time integration method

An implicit time marching with explicit subiterations was used in the calculations. The implicit solver can be written as

$$\frac{\beta_1(\vec{\hat{q}}V)^{n+1} + \beta_0(\vec{\hat{q}}V)^n + \beta_{-1}(\vec{\hat{q}}V)^{n-1}}{\Delta t} + \gamma_1\vec{R}(\vec{\hat{q}}^{n+1}) + \gamma_0\vec{R}(\vec{\hat{q}}^n) + \gamma_{-1}\vec{R}(\vec{\hat{q}}^{n-1}) = 0 \quad (3\text{-}10)$$

where $\vec{\hat{q}}V$ denote the unknowns times the volume. The coefficients $\beta_1, \beta_0, \beta_{-1}$ and $\gamma_1, \gamma_0, \gamma_{-1}$ can be chosen to yield desired accuracy an stability. We have used

$$\begin{aligned} \beta_1 &= 1.5;\ \beta_0 = -0.2;\ \beta_{-1} = 0.5 \\ \gamma_1 &= 1.0;\ \gamma_0 = 0.0;\ \gamma_{-1} = 0.0 \end{aligned} \quad (3\text{-}11)$$

in all calculations presented in this report.

Introduce the pseudo time τ, denote the dependent variables $\vec{\hat{q}}^{n+1}$ by $\vec{\hat{q}}^*(\tau)$ and consider the problem

$$V^{n+1}\frac{d}{d\tau}\vec{\hat{q}}^* + \vec{R}^*(\vec{\hat{q}}^*) = 0 \quad (3\text{-}12)$$

where

$$\vec{R}^*(\vec{\hat{q}}^*) = \frac{\beta_1 V^{n+1}}{\Delta t}\vec{\hat{q}}^* + \gamma_1\vec{R}^*(\vec{\hat{q}}^*) + \vec{Q} \quad (3\text{-}13)$$

and

$$\vec{Q} = \beta_0(\vec{\hat{q}}V)^n + \beta_{-1}(\vec{\hat{q}}V)^{n-1} + \gamma_0\vec{R}(\vec{\hat{q}}^n) + \gamma_{-1}\vec{R}(\vec{\hat{q}}^{n-1}) \quad (3\text{-}14)$$

is a constant source term. As steady state in pseudo time is approached

$$\frac{d}{d\tau}\vec{\hat{q}}^* \to 0 \Rightarrow \vec{\hat{q}}^* \to \vec{\hat{q}}^{n+1} \quad (3\text{-}15)$$

Within each real time step, the set of ordinary differential equations (3-12) is solved using an explicit Runge-Kutta method.

With an explicit q-stage Runge-Kutta scheme, the ODE

$$\frac{dU}{dt} = F(U) \quad (3\text{-}16)$$

can be written

$$\begin{aligned} u^1 &= u^n + \alpha_1\Delta t F(u^n) \\ u^2 &= u^n + \alpha_2\Delta t F(u^1) \\ &.... \\ u^q &= u^n + \Delta t F(u^{q-1}) \\ u^{n+1} &= u^q \end{aligned} \quad (3\text{-}17)$$

The coefficients α_i determine the stability and the order of accuracy of the Runge-Kutta scheme. In this report a second order accurate 5 stage Runge-Kutta scheme is used. The following coefficients are used

$$\alpha_1 = 0.814;\ \alpha_2 = 0.191;\ \alpha_3 = 0.342;\ \alpha_4 = 0.574;\ \alpha_5 = 1 \tag{3-18}$$

3.3 Boundary conditions

As we can not handle an infinitely large domain in space we must use boundary conditions in order to limit the problem.

In this section we describe the so called characteristic boundary conditions in detail and briefly introduce the non-reflecting boundary conditions due to Giles [5].

3.3.1 Characteristic boundary conditions

In order to investigate the mathematical properties of the system of Euler equations, we write the equations in quasi-linear form. The quasi-linear form of the system of Euler equations (2-1) is

$$\frac{\partial U}{\partial t} + \vec{\tilde{A}} \cdot \vec{\nabla} U = 0 \tag{3-19}$$

or equivalently

$$\frac{\partial U}{\partial t} + \tilde{A}\frac{\partial U}{\partial x} + \tilde{B}\frac{\partial U}{\partial y} = 0 \tag{3-20}$$

where $\tilde{A}$, $\tilde{B}$ are the components of the Jacobian vector matrix $\vec{\tilde{A}} = (\tilde{A}, \tilde{B})$, see [4], and $U = (\rho, \rho u, \rho v, \rho E)^T$ is the conservative variables vector.

The eigenvalues of the matrix $\tilde{K} = \vec{\tilde{A}} \cdot \vec{\kappa} = A\kappa_x + B\kappa_y$, associated with an arbitrary direction of propagation $\vec{\kappa}$, define for a large part the behaviour of the solutions to the Euler equations. It is therefore essential to have a clear understanding of the so called characteristic properties, since they represent essential aspects of inviscid flows, namely the propagation of disturbances.

Wave-like solutions will exist if the eigenvalues of the matrix $\tilde{K} = \vec{\tilde{A}} \cdot \vec{\kappa}$, for arbitrary $\vec{\kappa}$, are real with linear independence of the corresponding left eigenvectors. Let $\lambda_{(j)}$ denote an eigenvalue of the matrix $\tilde{K}$, obtained from

$$\det\left|\lambda_{(j)}\bar{I} - \tilde{K}\right| = 0 \qquad j = 1, 2, 3, 4 \tag{3-21}$$

and the left eigenvectors $\tilde{l}^{(j)}$ be solutions of

$$\tilde{l}^{(j)}\tilde{K} = \lambda_{(j)}\tilde{l}^{(j)} \qquad j = 1, 2, 3, 4 \tag{3-22}$$

Hence with the vectors $\tilde{l}^{(j)}$ as rows in L^{-1} and $\Lambda = diag(\lambda_1, \lambda_2, \lambda_3, \lambda_4)$ equation (3-22) can be written as

$$L^{-1}\tilde{K} = \Lambda L^{-1} \tag{3-23}$$

A direct calculation of the two dimensional problem (3-21) gives the eigenvalues $\lambda_1, \lambda_2, \lambda_3, \lambda_4$, here in matrix form,

$$\Lambda = \begin{bmatrix} \lambda_1 & 0 & 0 & 0 \\ 0 & \lambda_2 & 0 & 0 \\ 0 & 0 & \lambda_3 & 0 \\ 0 & 0 & 0 & \lambda_4 \end{bmatrix} = \begin{bmatrix} u & 0 & 0 & 0 \\ 0 & u & 0 & 0 \\ 0 & 0 & u+c & 0 \\ 0 & 0 & 0 & u-c \end{bmatrix} \tag{3-24}$$

were c is the speed of sound.

The so called compatibility equations, see [4], for the eigenvalues Λ one can write in a compact form as

$$(L^{-1}\partial_t + L^{-1}\vec{A}\cdot\vec{\nabla})U = 0 \tag{3-25}$$

These equations lead to the introduction of the characteristic variables. They are defined as a 4×1 column vector by the relation valid for arbitrary variations δ (either ∂_t or $\vec{\nabla}$):

$$\delta W = L^{-1}\delta V \tag{3-26}$$

The compatibility equation can now be expressed as

$$L^{-1}\frac{\partial V}{\partial t} + (L^{-1}\vec{A}L)L^{-1}\vec{\nabla}V = 0 \tag{3-27}$$

At a boundary in a multi-dimensional flow the one-dimensional analysis gives insight to the number and type of boundary conditions that should be used. This is since it is the eigenvalue spectrum associated with the normal to the boundary that decides the number and type of boundary conditions.

The characteristic form of the one-dimensional Euler equations can be written as

$$\frac{\partial W}{\partial t} + \Lambda\frac{\partial W}{\partial x} = 0 \tag{3-28}$$

since in one dimension $\vec{A} = \tilde{K}$.

Applying the definition (3-26) for a one-dimensional flow, the following definition of the characteristic variables $\delta W = (\delta w_1, \delta w_2, \delta w_3)^T$, with δW representing an arbitrary variation, either ∂_t or ∂_x, are obtained from $\delta W = L^{-1}\delta V$:

$$\begin{aligned} \delta w_1 &= \delta\rho - \frac{1}{c^2}\delta p \\ \delta w_2 &= \delta u - \frac{1}{\rho c}\delta p \\ \delta w_3 &= \delta u + \frac{1}{\rho c}\delta p \end{aligned} \tag{3-29}$$

Using the characteristic variables, or equivalently the Riemann invariants, is a staightforward way to express the propagation properties in a one-dimensional flow. Equation (3-28) shows that the quantities w_j propagate along the corresponding characteristics with the speed $\lambda_{(j)}$. Hence δw_1 in (3-29) propagates with velocity $\lambda_1 = u$ along the characteristic C_0 defined by $\mathrm{d}x/\mathrm{d}t = u$. This characteristic is the path line of the fluid. On the other hand, δw_2 propagates with velocity $\lambda_2 = u + c$ along the characteristic C_+ defined by $\mathrm{d}x/\mathrm{d}t = u + c$ and δw_3 propagates with velocity $\lambda_3 = u - c$ along the characteristic C_- defined by $\mathrm{d}x/\mathrm{d}t = u - c$.

The characteristics C_0 and C_+ have slopes $u + c$ and u, which are always positive for a flow in the positive x direction. The third characteristic C_- has a slope $u - c$ whose sign depends on the Mach number. For subsonic flow, C_- will have a negative slope but a positive slope for a supersonic flow. See Fig. (3-1).

Fig. 3-1. Boundary conditions for one-dimensional inviscid flows.

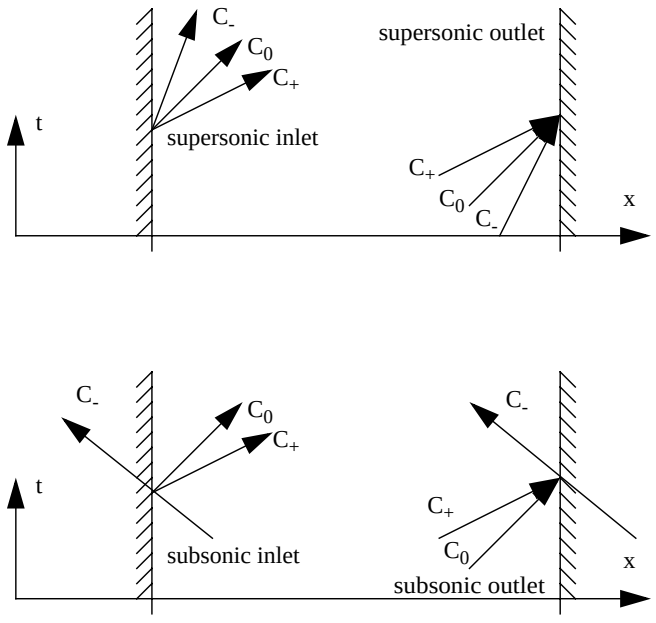

The number of boundary conditions to be imposed will depend on the sign of the slope of the characteristics at the boundaries. Only variables transported from the boundaries towards the interior can be freely imposed at the boundaries as physical boundary conditions, see e.g. [6]. Numerical boundary conditions will have to be added to the physical conditions in order to completely define the numerical problem. Table (3-1) shows the number and the nature of the boundary conditions.

Tab. 3-1. Physical and numerical boundary conditions for one-dimensional flows.

	Subsonic	Supersonic
Inlet	*Physical conditions: w_1, w_2* *Numerical conditions: w3*	*Physical conditions: w_1, w_2, w3* *Numerical conditions: none*
Outlet	*Physical conditions: w3* *Numerical conditions: w1, w2*	*Physical conditions: none* *Numerical conditions: w1, w2, w3*

In this report we consider a subsonic inflow, why w_1 and w_2 are physical conditions and w_3 is a numerical condition.

At the inflow boundary we use these characteristic boundary conditions, while we use a non-reflecting boundary condition, see Sec. 3.3.2, at the outflow boundary.

Figure (3-2) shows the discretization near the boundary. The first cell to the left represents the dummy cell variables. Cell 2 and 3 are the first and second cell inside the computational domain, respectively. B is the specified solution on the boundary of the domain.

Fig. 3-2. Discretization near the boundary.

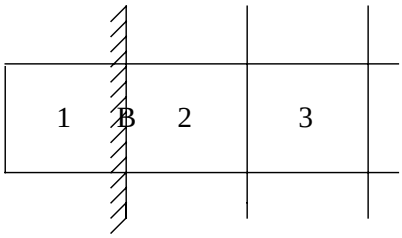

We have characteristics C_0 and C_+ that are propagating into the domain and will be given by

$$w_{i,B} = \frac{w_{i,1} + w_{i,2}}{2} \qquad i = 1, 2 \tag{3-30}$$

while we have an outgoing characteristic C_- which is received through a first-order extrapolation as

$$w_{i,1} = 2w_{i,2} - w_{i,3} \qquad i = 3 \tag{3-31}$$

The tangential velocity is assumed to be constant across the boundary.

3.3.2 Non-reflecting boundary conditions

As we actually have an infinite domain which is truncated to a finite domain, it rises the problem of choosing appropriate boundary conditions for the far-field boundary. Ideally these should prevent any non-physical reflection of outgoing waves

We have used Giles second order non-reflecting boundary conditions [5] at the outflow boundary.

In [5], the non-reflecting boundary conditions are derived for a linearized problem. In this study we linearized around the jet flow described by Eqn. (2-5) to (2-8).

We used the so called second order two-dimensional unsteady outflow boundary condition, which is

$$\frac{\partial c^4}{\partial t} + (0 \quad u \quad 0 \quad v)\frac{\partial}{\partial y}\begin{pmatrix} c_1 \\ c_2 \\ c_3 \\ c_4 \end{pmatrix} = 0 \tag{3-32}$$

and linear extrapolation of the outgoing characteristics $c_i \quad i = 1, 2, 3$.

Here $c_i \quad i = 1, 2, 3, 4$ are the amplitudes of the four characteristic waves found as

$$\begin{bmatrix} c_1 \\ c_2 \\ c_3 \\ c_4 \end{bmatrix} = \begin{bmatrix} -c^2 & 0 & 0 & 1 \\ 0 & 0 & \rho c & 0 \\ 0 & \rho c & 0 & 1 \\ 0 & -\rho c & 0 & 1 \end{bmatrix} \begin{bmatrix} \delta\rho \\ \delta u \\ \delta v \\ \delta p \end{bmatrix} \tag{3-33}$$

where $\delta\rho, \delta u, \delta v$ and δp are the perturbations from the jet flow around which the Euler equations are linearized.

4 Numerical results

Throughout the calculations the following parameter values were used: The free stream values were $p_\infty = 101000$, $T_\infty = 288$, $u_\infty = 100$ and $v_\infty = 0$. For the jet input (2-5), (2-6) we used $a = 75$, $T_\infty / T_c = 1/2$, $u_\infty / u_c = 1/4$, $M_c = 0.8$ and $\gamma = 1.4$.

The free stream values yield a subsonic flow, since the eigenvalue $u - c$ will be negative trough out the flow, see Fig. 4-1. Here the speed of sound c is defined as $c = \sqrt{\gamma R_{gas} T}$ where $R_{gas} = 287$.

The computational domain is represented by a rectangle with height $H = 0.2$ and length $L = 0.2$, see fig. (2-1).

Fig. 4-1. Eigenvalue $u - c$ when $u_\infty = 100$.

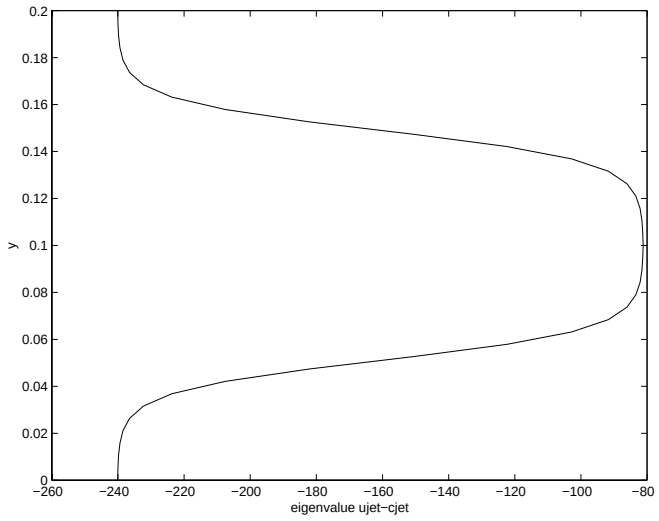

4.1 Initial data

As initial data we used the jet flow described by (2-5) through (2-8) in the whole domain. Figure (4-2) shows the structure of the density in the initial data.

Fig. 4-2. Structure of the density.

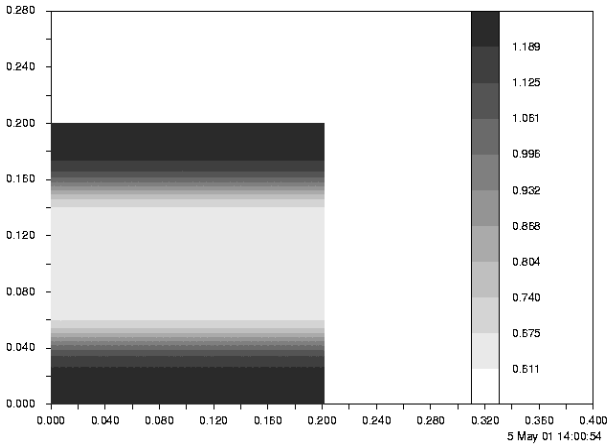

We used a time step $\Delta t = 4.573 \cdot 10^{-6}$ and all calculation were performed in double precision. Here the step in x-direction is $\Delta x = 0.0025$ and the step in y-direction is $\Delta y = 0.0025$.

Firstly we ran the program without acoustic input in order to numerically check the solution, (2-5)-(2-7). After a few time steps instabilities were noted in the pressure and the velocity fields (Fig. 4-3). One could also see a disturbance near the inflow boundary, mainly were there where large gradients. The instabilities were generated in the beginning of a calculation and then moved downstream with the particle velocity. A possible source of these instabilities could be the initial data. Otherwise instabilities would probably have been generated continuously during the calculation. The instabilities were only seen in the pressure and velocity fields.

Fig. 4-3. Pressure instability.

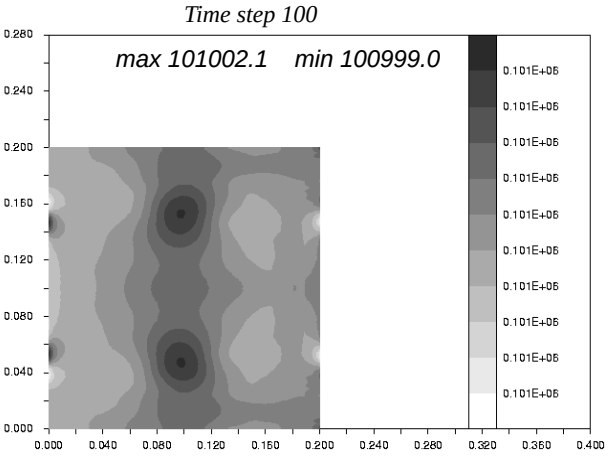

Since the instabilities were locally generated in time, a satisfying solution would have been achieved as soon as the instabilities had passed through the outflow boundary. However even with a non reflecting boundary condition the instabilities were severely reflected, see Fig. (4-4). The same result was obtained with boundary conditions where all variables were extrapolated. The reflections from

the instabilities were then growing as they travelled up-stream after the reflection at the outflow boundary.

Fig. 4-4. Reflection at the outflow boundary.

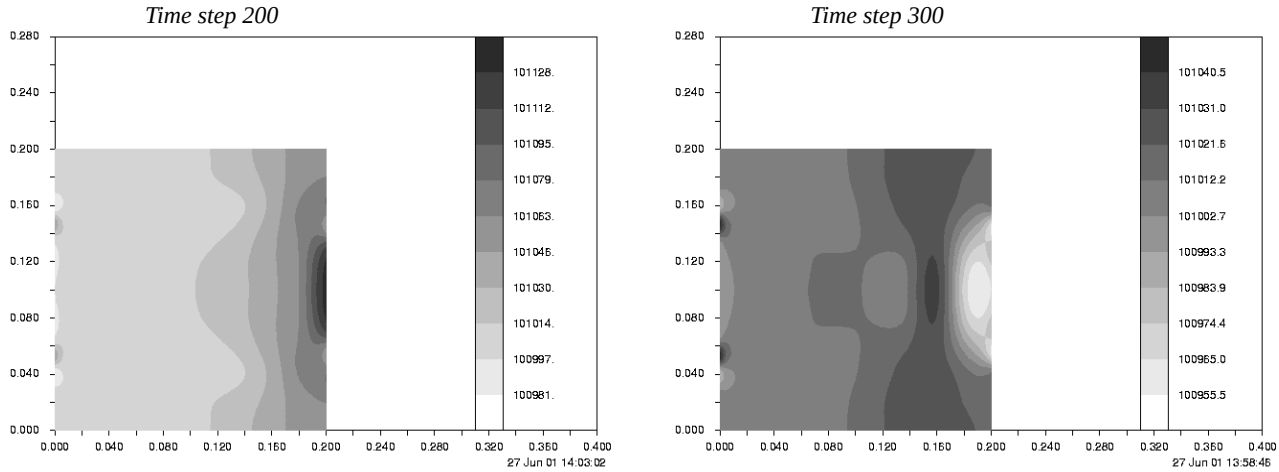

The instabilities have just reached the outflow boundary. *Reflection of the instabilities*

It should be note that the acoustic waves will have an amplitude of about 100 Pa, and hence a disturbance of the same order as the acoustic wave is not acceptable.

We also tried a different indata file. It was constructed with data (u, v, w, ρ, p) from a calculation described above for a fixed x for which the instability already had passed but to which reflections from the boundary had not yet reached. However it turned out that the instability problem remained also with this initial data.

We thereafter made experiments with the grid, artificial viscosity coefficients and outflow boundary conditions in order to reduce the amplitude of the instabilities as they reached the outflow boundary.

First experiments with the grid were made. Firstly, we tried to damp the oscillations by adding extra layers of cells in the x-direction. Two different grid sizes were tested. The first grid was extended with 13 extra cells in x-direction and the other one was extended with 16 extra cells in x-direction. The first six cells had the same size as the original grid, thereafter they increased by a factor 1.4, see Fig. 4-5.

It could be seen that the amplitude of the pressure disturbance reduced in both cases but the instability wasn't totally reduced for any of the grids. Since the longer grid had much wider cells at the end than the shorter grid, we expected the instability to have smaller amplitude with the longer grid when the instability reached the outflow boundary. Instead the shorter grid showed to give a smaller increase in pressure.

Fig. 4-5. Structure of the grid extension.

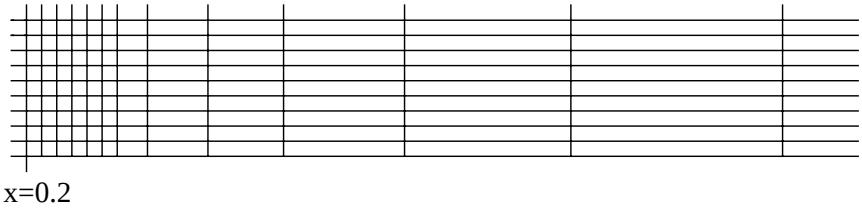

During this grid test, small oscillations due to dispersion could bee seen in the solution. However, when increasing the viscosity parameters the boundary layer at the outflow boundary increased, see Fig. 4-6 and 4-7. The most noticeable effect of increasing the viscosity parameters was seen when the longer grid was used.

This effect can be seen from the solution of the viscous one-dimensional model problem

$$\begin{aligned} u_x &= \varepsilon u_{xx} \\ u(x) &\to 0 \ \text{ as } \ x \to -\infty \\ u(1) &= u_0 \end{aligned} \tag{4-1}$$

with the solution $u = u_0 e^{\frac{(x-1)}{\varepsilon}}$. It is clearly seen that the boundary layer at the outflow boundary is thicker with a larger value of ε.

Fig. 4-6. Result of the viscosity test.
$\kappa^{(2)} = 1.0 \quad \kappa^{(4)} = 0.1$

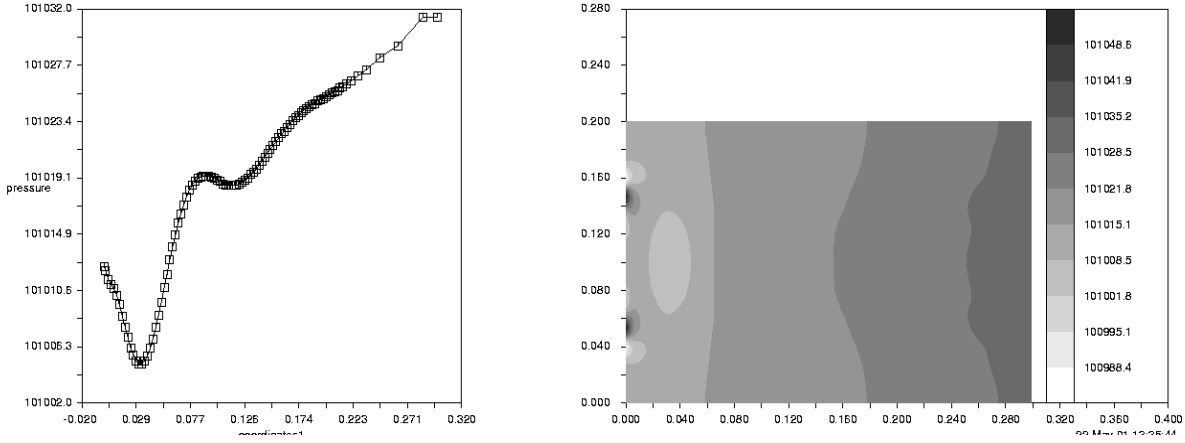

Fig. 4-7. Result of the viscosity test.
$\kappa^{(2)} = 0.05 \quad \kappa^{(4)} = 0.005$

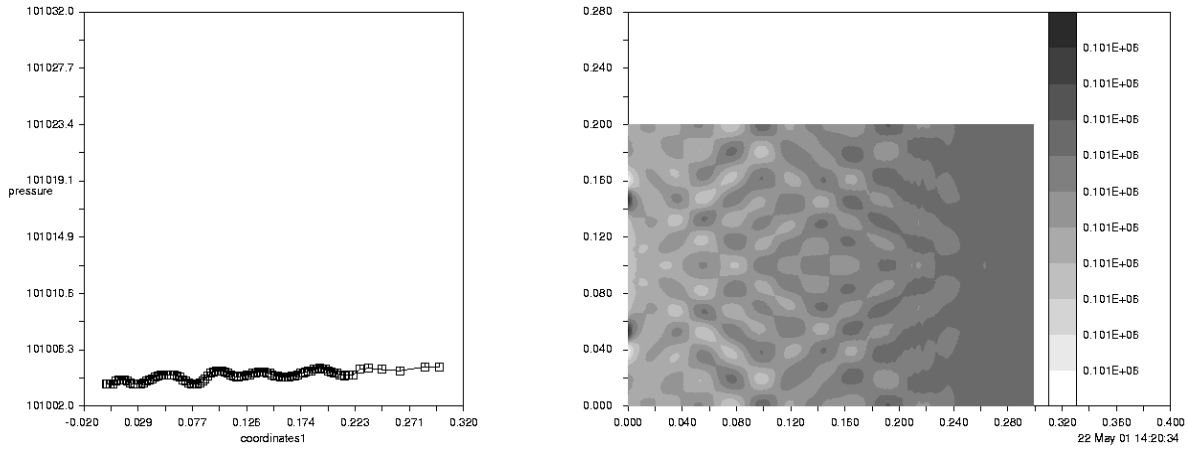

In this study we also compared different outflow boundary conditions; imposing pressure, extrapolation of all variables and the non-reflecting boundary conditions described in section 3.3.2.

With the extended grid all boundary conditions gave well-behaved solutions. See Fig. 4-8 - 4-10. Before the extension of the grid was made the instabilities were reflected when the non-reflection boundary condition was used (Fig. 4-4). Now, on the enlarged grid, the frequencies became smaller which seemed to help the non reflecting boundary condition to let the instabilities out (Fig. 4-10). In Fig. 4-8 to 4-10 the maximum and minimum values are given for $0 < x < 0.319$ when $\kappa^{(2)} = 1.0$, $\kappa^{(4)} = 0.1$ were used.

In Table 4-1 the maximum an minimum values, respectively, are shown for $0 < x < 0.2$ for the three different boundary conditions tested.

Fig. 4-8. Imposed pressure.

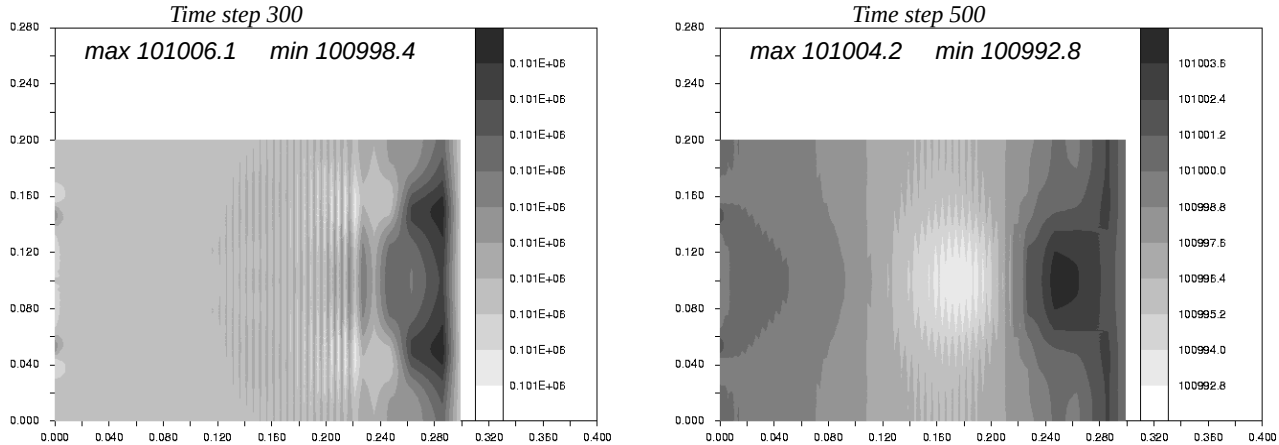

Fig. 4-9. Extrapolation of variables.

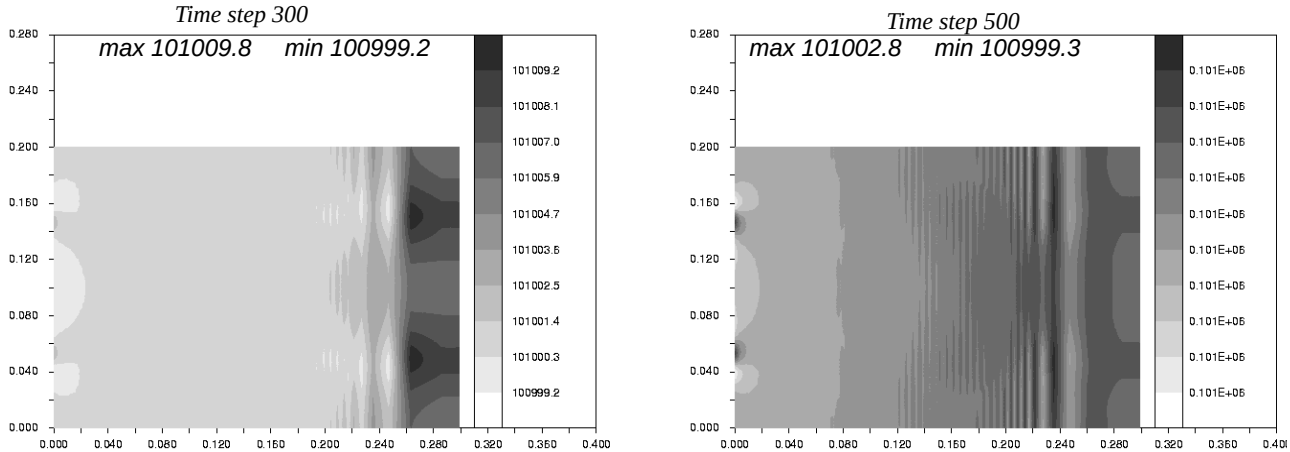

Fig. 4-10. Non-reflecting boundary condition.

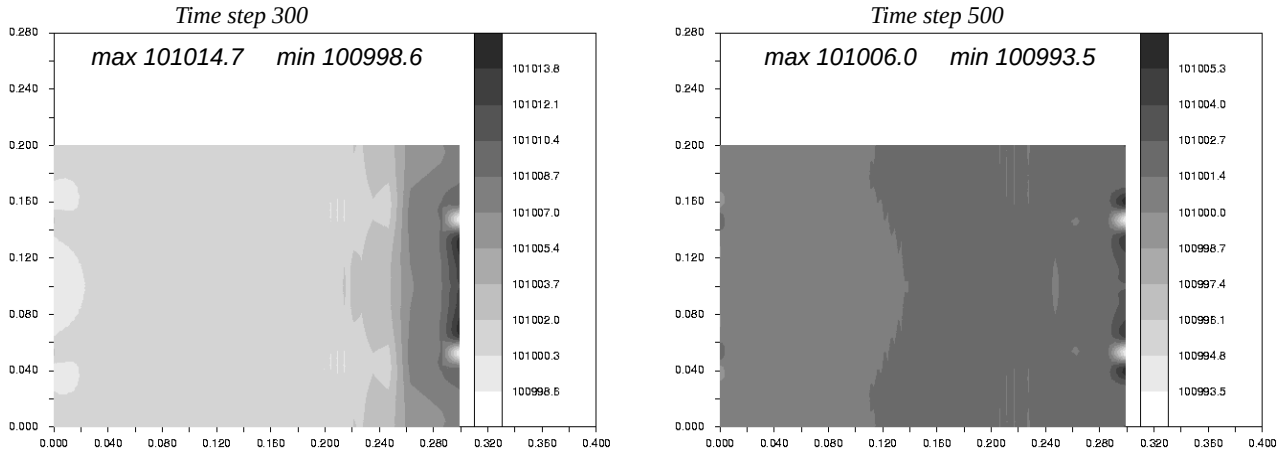

In table 4-1 maximum and minimum values when $0 \le x \le 0.2$ are shown.

Tab. 4-1. Maximum and minimum values when $0 \le x \le 0.2$.

Time step		Imposed pressure	Extrapolation of variables	Non-reflecting boundary cond.
300	max	101002.2	101002.2	101002.2
	min	100998.8	100999.2	100999.2
500	max	101002.0	101002.4	101002.6
	min	100992.8	100999.3	100999.4

The conclusion is that a grid with a short extension and small values of the viscosity parameters gave the best reducing effect on the instabilities. The choice of boundary condition had no noticeable effect on the solution.

4.2 Acoustic calculations

Here we used a solution, as described in Sec. 4.1, generated with a grid extension by 13 extra cells, the viscosity parameters $\kappa^{(2)} = 1.0$ $\kappa^{(4)} = 0.1$ and a non-reflecting boundary condition as initial data.

An acoustic wave as in Sec. 2.2 was superimposed to the data at the inflow boundary. In this report only downstream travelling acoustic waves are considered.

In section 4.1 it was shown that small values of the viscosity parameters gave the best initial data to the inviscid problem. The same viscosity test were also made in the acoustic case. The smaller values did however give rise to oscillations, see Fig. 4-11 and 4-12.

Fig. 4-11. Pressure for $y = 0.05$. Time step 600.

$\kappa^{(2)} = 1.0$ $\kappa^{(4)} = 0.1$ $\kappa^{(2)} = 0.05$ $\kappa^{(4)} = 0.005$

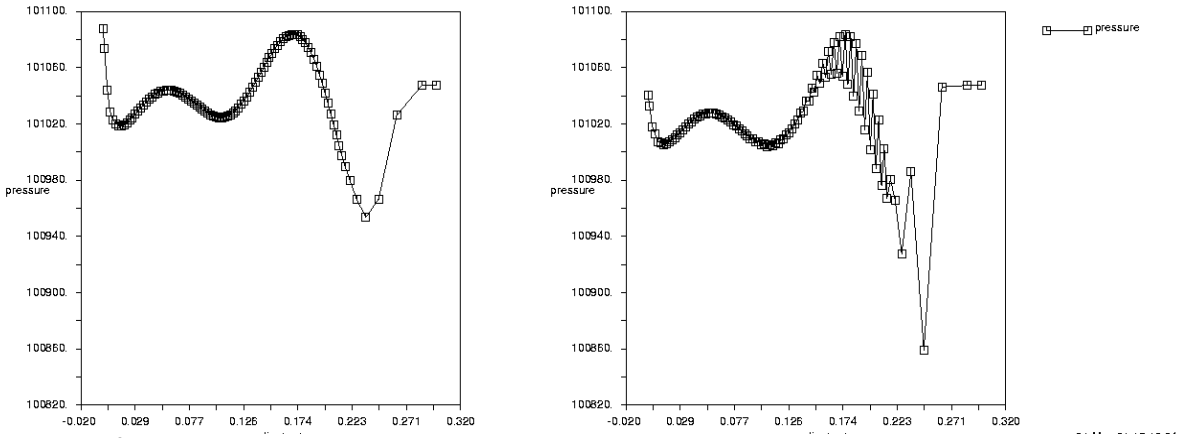

Fig. 4-12. Pressure for $y = 0.05$. Time step 600.

$\kappa^{(2)} = 1.0$ $\kappa^{(4)} = 0.1$ $\kappa^{(2)} = 0.05$ $\kappa^{(4)} = 0.005$

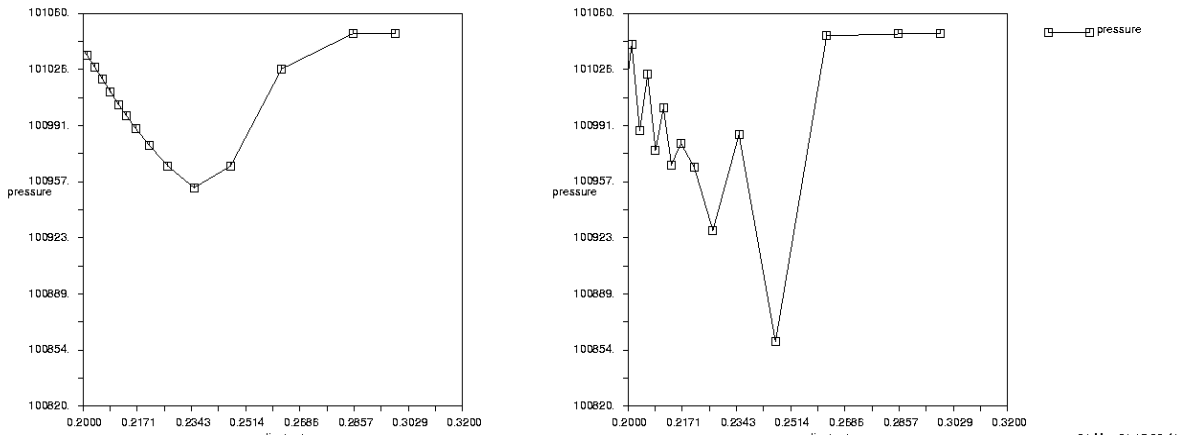

The purpose of the following calculations was to investigate how many grid points that had to be used in order to propagate the acoustic waves in a non-homogenous medium.

Three grids with different number of grid points where constructed, namely 48×41, 94×81 and 186×161. The different results of three acoustic parameters were compared. The different parameters where: The amplitude of the disturbance p_0, the cut off ratio ξ and the number of grid points in y-direction N_y. A standard set of input parameters, that was arbitrarily chosen (case 1 in table 4-2), was used as a reference. Only one of the standard input parameters were changed for each comparison. The different parameters that were tested is shown in table 4-2. Each case was tested for $N_y = 40, 80$ and 160.

Tab. 4-2. Parameters for different test cases.

	case 1*	case 2	case 3	case 4	case 5	case 6
ξ	1.1	0.7	0.9	1.5	1.1	1.1
p_0	89	89	89	89	50	130

* Case 1 is the reference set of input parameters

We used

$$\Delta t = \frac{t}{60} \tag{4-2}$$

where

$$T = \frac{2\pi}{\omega_\infty} \tag{4-3}$$

and

$$\omega_\infty = \xi c_\infty k_y \sqrt{1 - \bar{M}_\infty^{\,2}} \tag{4-4}$$

The free stream values of c_∞ and M_∞ will give the greatest value of ω and hence they will be used in the calculation of Δt.

Also,

$$k_y = \frac{2\pi}{N_y \Delta y} \tag{4-5}$$

For this problem $\Delta t = \frac{T}{60}$ was chosen why a time step, $\Delta t = 4.573 \cdot 10^{-6}$, will be satisfying for every test case.

In figure 4-13 through 1 the solution for case 1 to 6 are shown for $N_y = 40, 80 \text{ and } 160$ at time step 1000. The behaviour of the solution for $x > 0.2$, i.e. a the extra layers of cells added for damping of reflections at the outflow boundary, is neglected in the comparisons.

By comparing the structure of the solutions with different N_y for each case one can see that with $N_y = 80$ and $N_y = 160$ we get fairly similar results but not enough to use $N_y = 80$. The conclusion will therefore be that $N_y = 160$ is needed for an accurate solution. This particular problem is however difficult due to the very large gradients of the jet flow.

Fig. 4-13. Case 1,
$N_y = 40$.

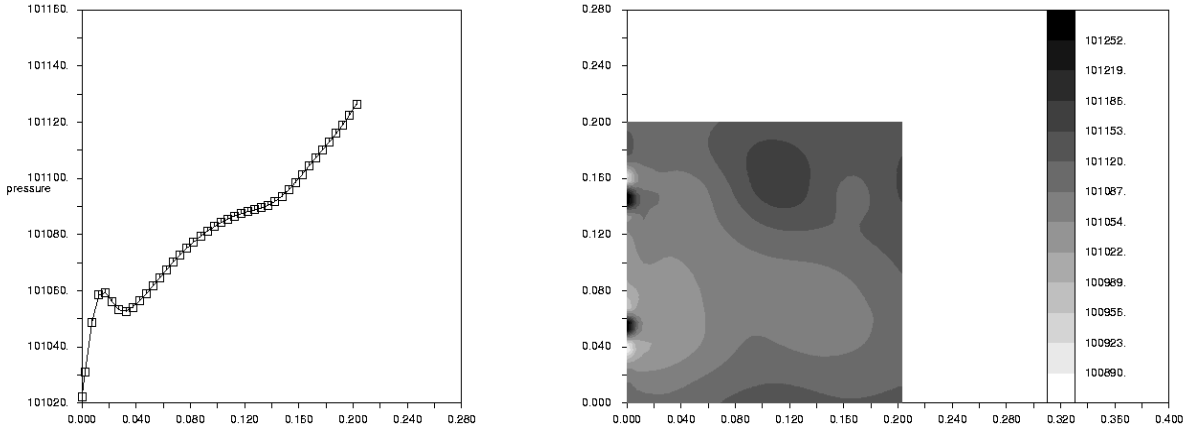

Fig. 4-14. Case1,
$N_y = 80$.

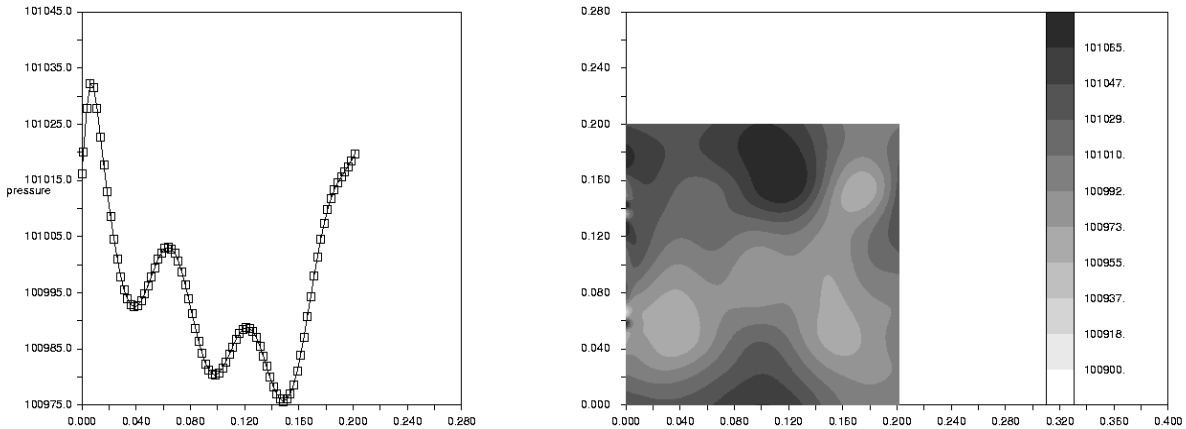

Fig. 4-15. Case1,
$N_y = 160$.

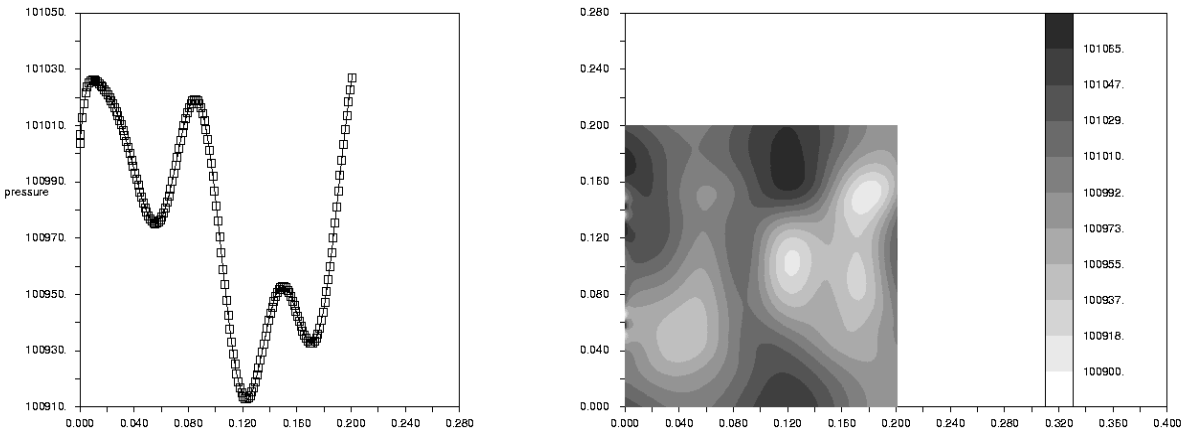

Fig. 4-16. Case 2,
$N_y = 40$.

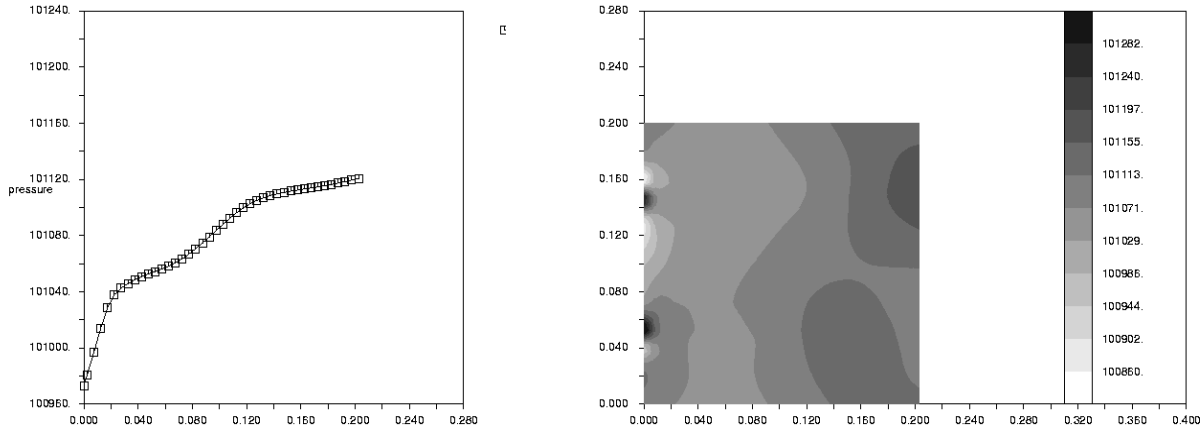

Fig. 4-17. Case 2,
$N_y = 80$.

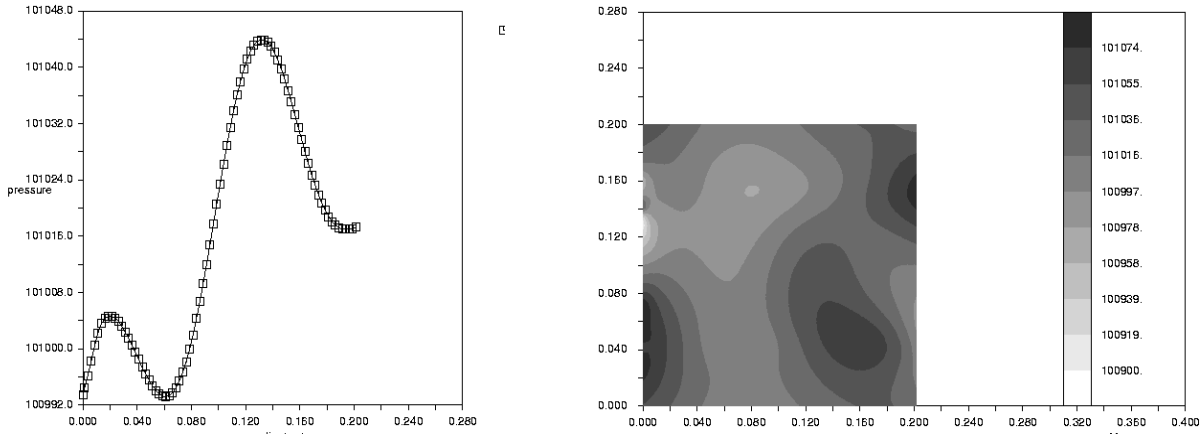

Fig. 4-18. Case2,
$N_y = 160$.

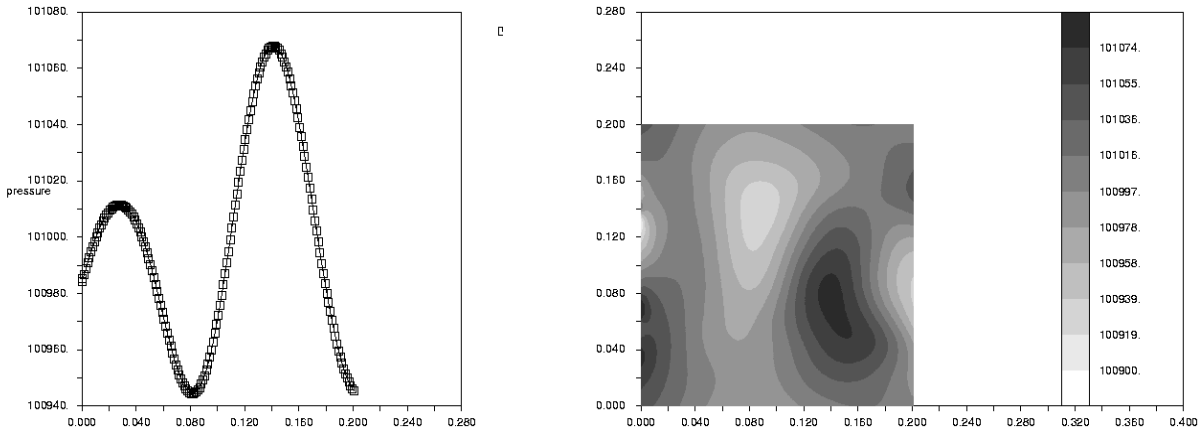

Fig. 4-19. Case 3,
$N_y = 40$.

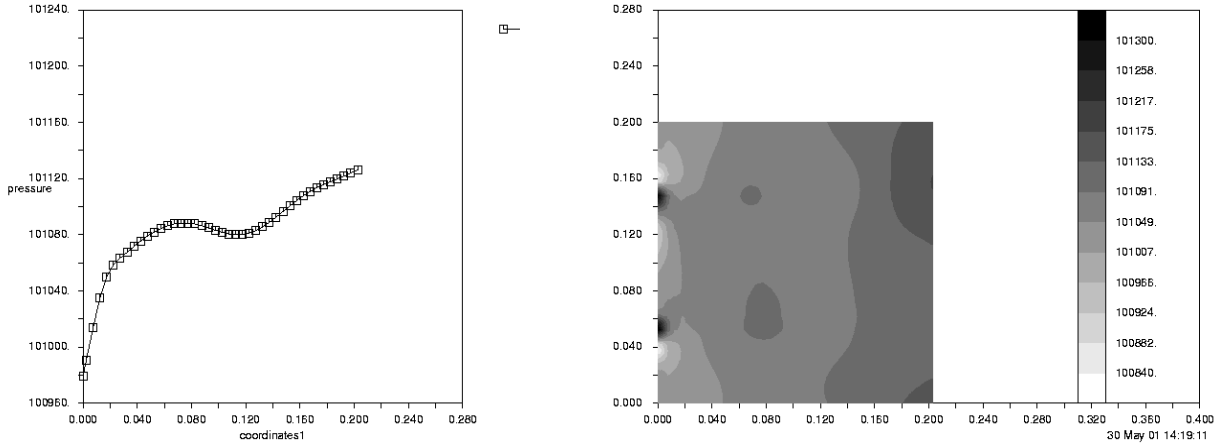

Fig. 4-20. Case3,
$N_y = 80$.

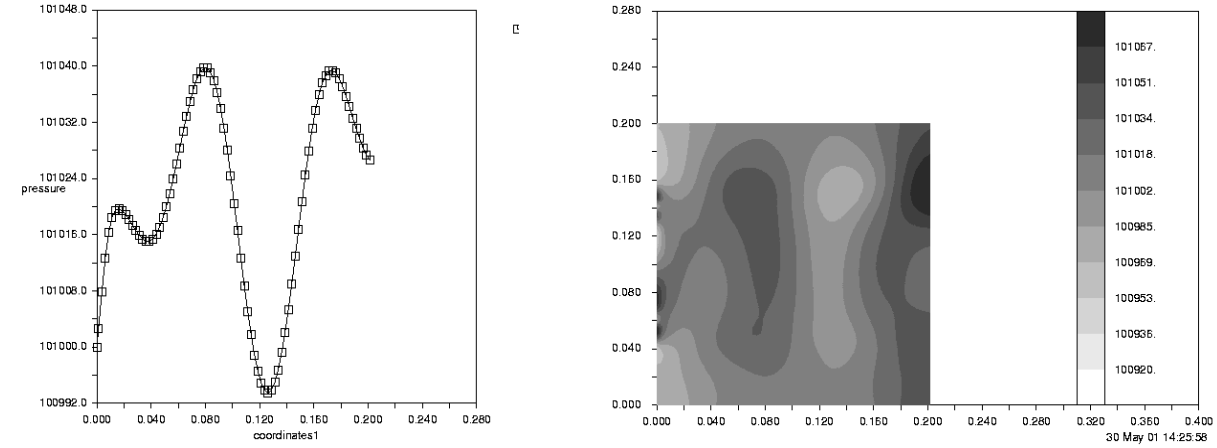

Fig. 4-21. Case 3,
$N_y = 160$.

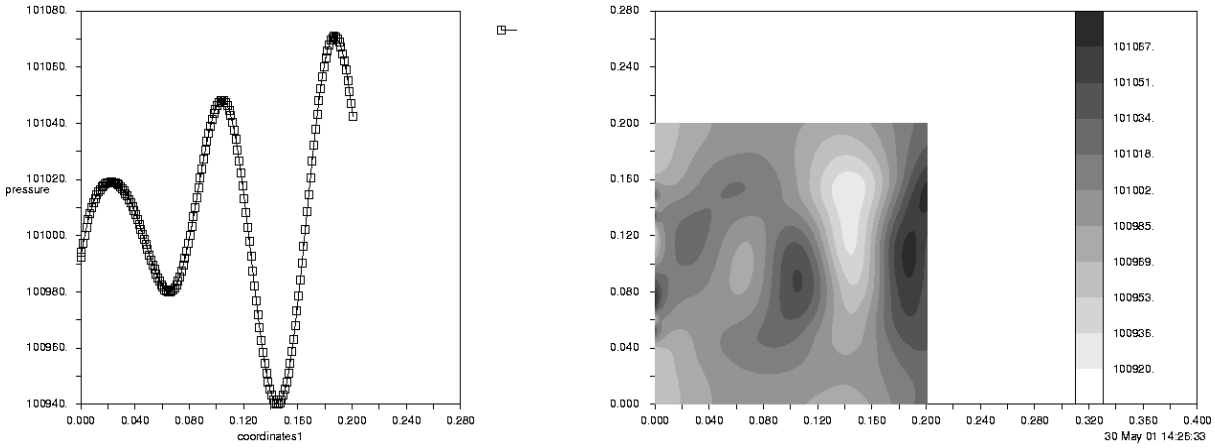

Fig. 4-22. Case 4,
$N_y = 40$.

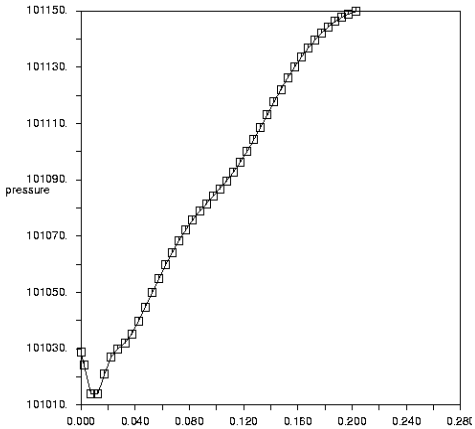

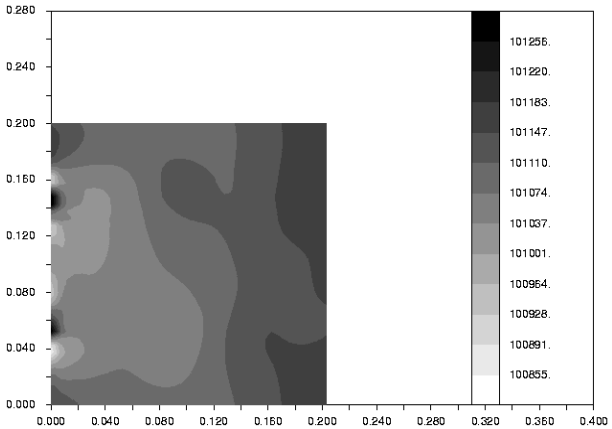

Fig. 4-23. Case4,
$N_y = 80$.

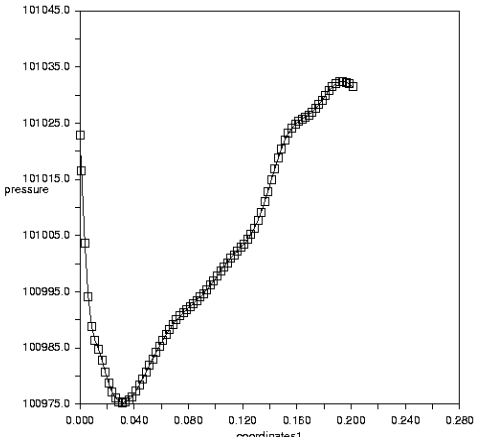

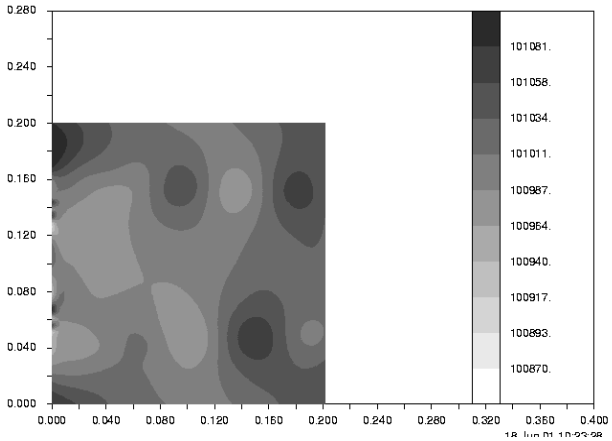

Fig. 4-24. Case4,
$N_\theta = 160$.

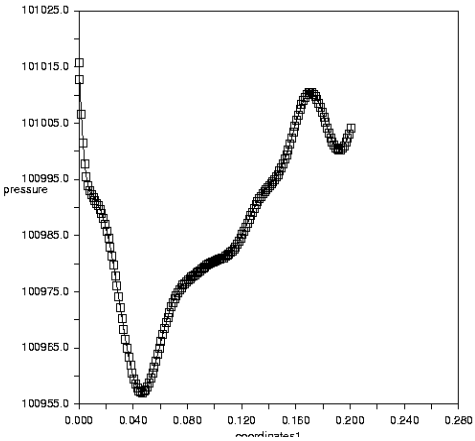

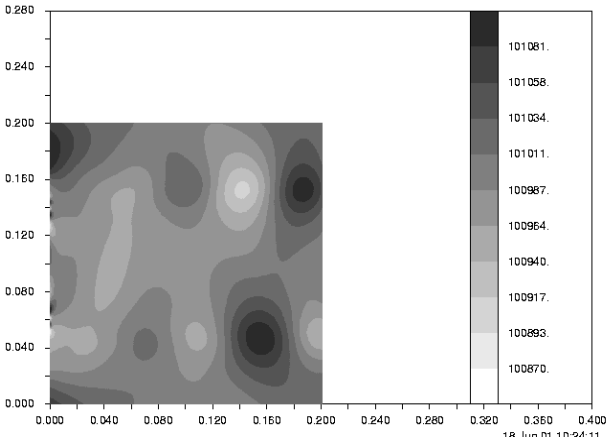

Fig. 4-25. Case 5,
$N_y = 40$.

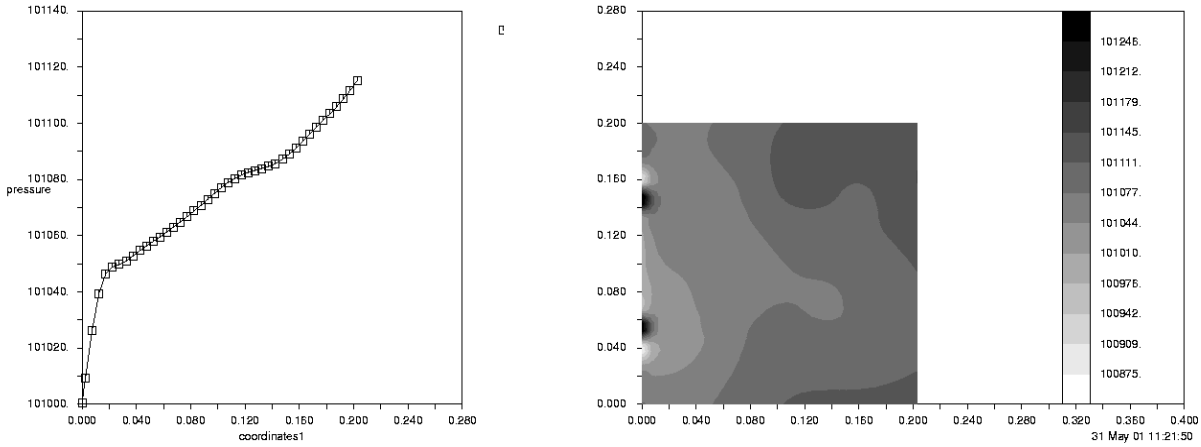

Fig. 4-26. Case5,
$N_y = 80$.

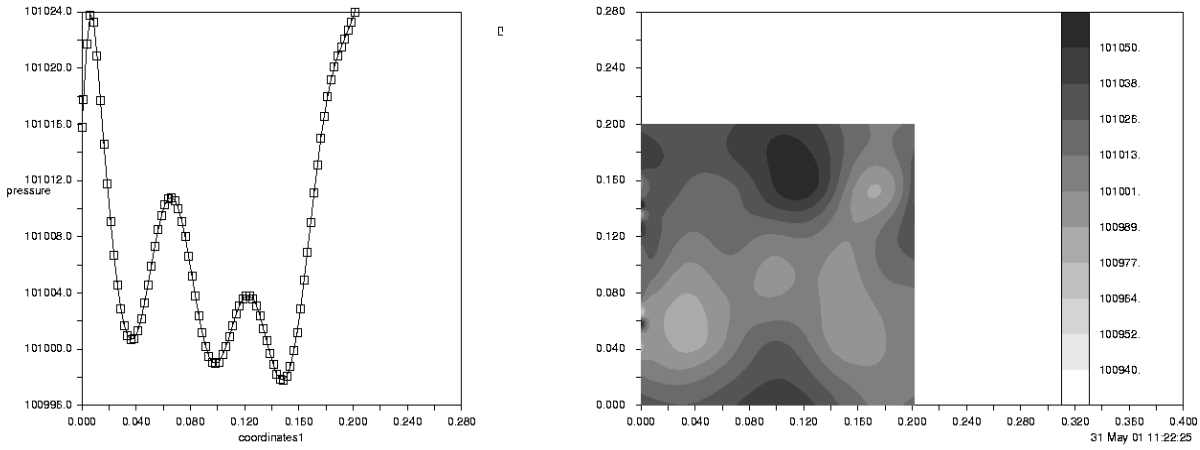

Fig. 4-27. Case5,
$N_y = 160$.

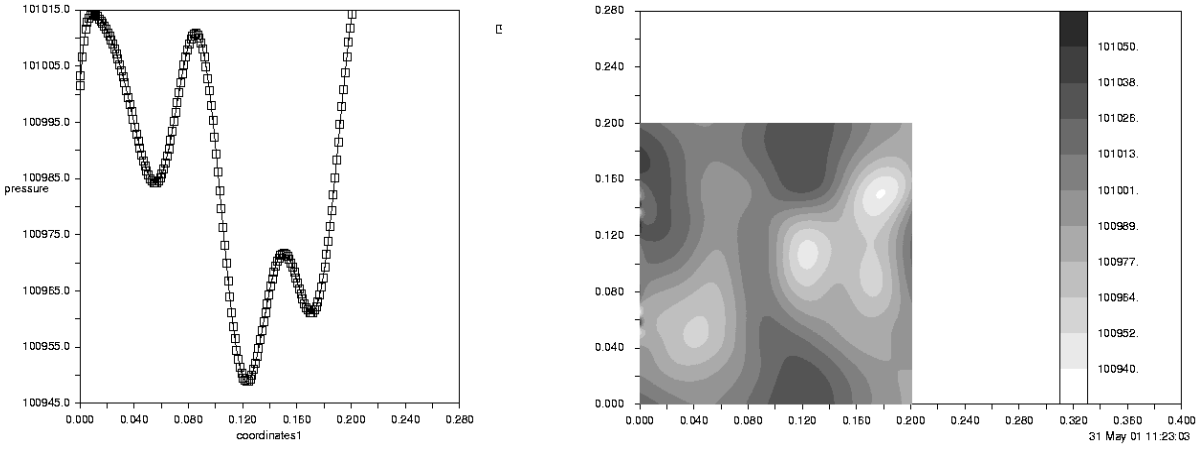

Fig. 4-28. Case 6,
$N_y = 40$.

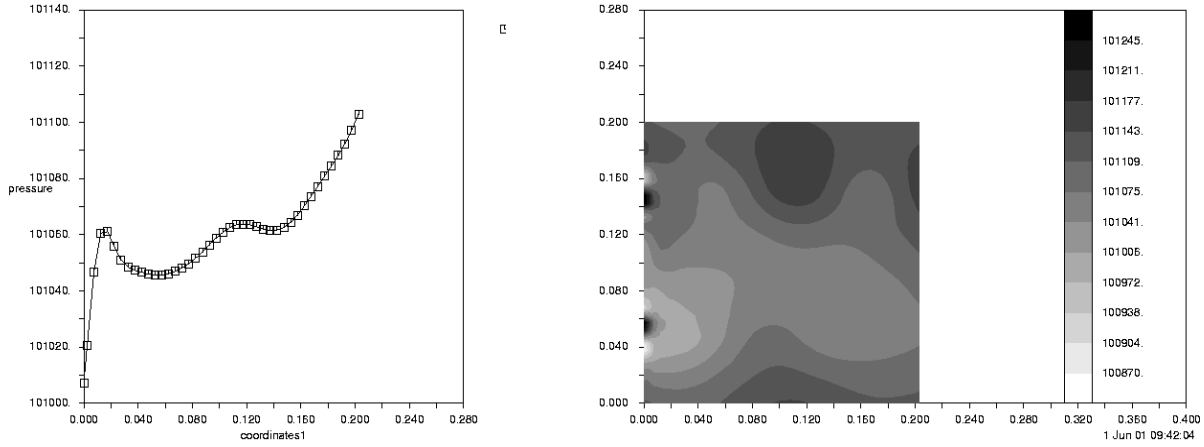

Fig. 4-29. Case6,
$N_y = 80$.

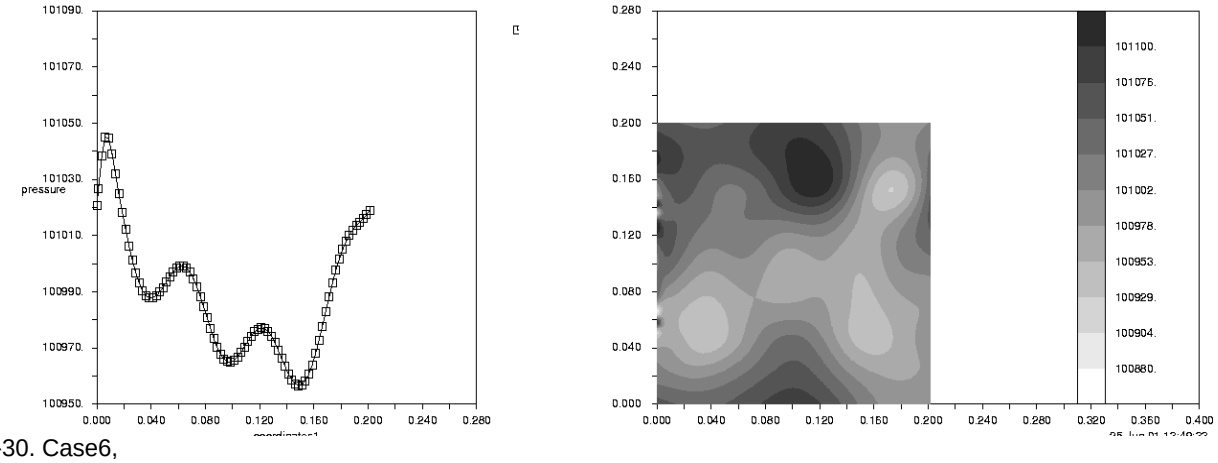

Fig. 4-30. Case6,
$N_y = 160$.

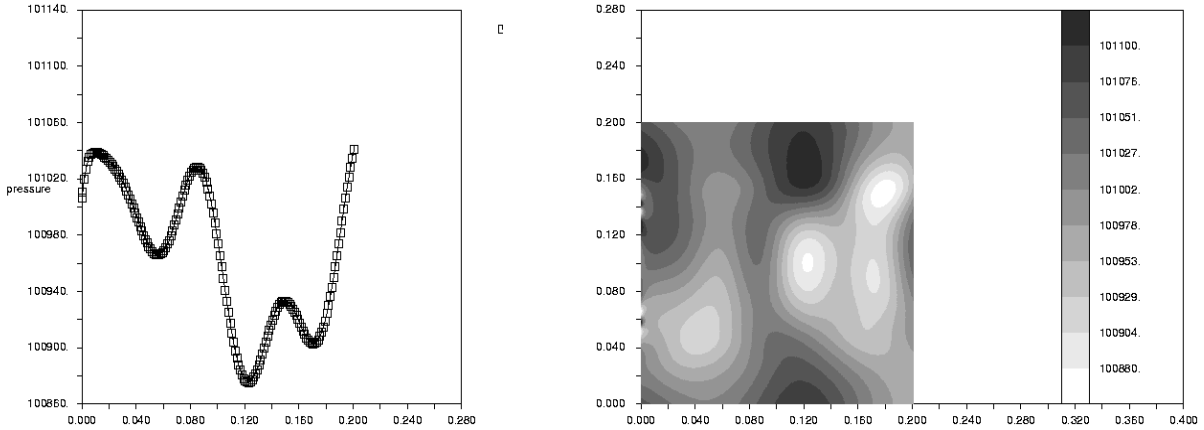

5 Summery

A numerical study was performed to investigate the performance of a second order accurate finite volume solver when the solution contained acoustic waves spreading in air with non-constant speed of sound. A two dimensional model was set up with a subsonic jet flow as base flow and an acoustic wave was superimposed.

It was theoretically and numerically verified that the jet flow model that was used satisfied the Euler equations. In the numerical verification instabilities appeared in the pressure and velocity fields. Since the instabilities were reflected at the outflow boundary and hence would destroy the calculations including acoustic waves, attempts were made to reduce the magnitude of the instabilities before they reached the outflow boundary. Tests were made by changes in indata, grid size, viscosity parameters and boundary conditions.

In the acoustic calculations different viscosity parameters were tested. Examination of how many grid points that had to be used in order to propagate the acoustic waves in a non-homogenous medium was made. The examination was performed by comparing six cases, all with different values of cut off ratio, number of grid points in y-direction and amplitude of the disturbance.

After the inviscid calculations turbulent calculations were initiated. Satisfying boundary data of the turbulent quantities were however hard to obtain. An attempt to achieve a fair guess of the turbulent quantities was performed as follows. The pressure, velocities and density was fixed to the jet values. Also, the problem was considered as periodic also in the x-direction. The intention was that the turbulent quantities should after integrating in time reach a steady state solution. However, with different guesses of the initial solution of the turbulent quantities no sign of convergence were noted although over 100.000 time steps were taken.

References

[1] K. Jensen, G. Efraimsson, “Aero Engine Fan Noise Resolution Requirement in Computational Fluid Dynamics”, Scientific report FOI in preparation.

[2] M.E. Hayder, E. Turkel and R.R. Mankabadi, “Numerical Simulation of a High Mach Number Jet”, AIAA paper 93-0653

[3] A. Rizzi, P. Eliasson, I. Lindblad, C. Hirsch, C. Lacor and S. Häuger, “The Engineering of Multiblock/Multi-grid Software for Navier-Stokes Flows on Structured Meshes”, Computers Fluids, vol. 22 pp 341-367, 1993.

[4] C. Hirsch, “Numerical Computation of Internal and External Flows” Volume 2: Computational Methods for Inviscid and Viscous Flows, John Wiley and sons, 1990.

[5] M. Giles, “Non-Reflecting Boundary Conditions for the Euler Equations”, Computational Fluid Dynamics Laboratory, Department of Aeronautics and Astronautics, Massachussetts Institute of Technology, CFDL-TR-88-1, 1988.

[6] H.-0. Kreiss, J. Lorenz, “Initial-Boundary Value Problems and the Navier-Stokes Equations”, Academic Press, 1989.

Issuing organization
FOI-Swedish Defence Research Agency
Division of Aeronautics, FFA
SE-172 90 STOCKHOLM

Report number, ISRN
FOI-R--0243--SE

Report type
Scientific report

Month year
November 2001

Project number
C840234

Customer code
3. Aeronautical Research

Research area code
7. Vehicles

Sub area code
73. Aeronautical Research

Author(s)
Åsa Hetyei
Gunilla Efraimsson

Project manager
Gunilla Efraimsson

Approved by
Torsten Berglind
Head, Computational Department

Scientifically and technically responsible
Gunilla Efraimsson
Computational Department

Report title
A numerical study of acoustic waves in a non-homogeneous flow

Abstract
A numerical study of acoustic waves propagating in a non homogeneous flow was performed on a two dimensional domain. A subsonic jet flow was used as a base flow to which an acoustic wave was superimposed. It was theoretically and numerically verified that the jet flow model that was used satisfied the Euler equations. In the numerical verification instabilities appeared in the pressure and velocity fields. Since the instabilities were reflected at the outflow boundary and hence would destroy the calculations including acoustic waves, attempts were made to reduce the magnitude of the instabilities before they reached the outflow boundary. Examination of how many grid points that had to be used in order to propagate the acoustic wave in a non-homogenous medium was made.

Keywords
Aero acoustics, jet flow, non-reflective boundary conditions

Further bibliographic information
Master thesis

ISSN
ISSN 1650-1942

Pages
46

Language
English

Distribution according to missiv

Price
Price acc. to price list

Security classification
Unclassified

Utgivare	Rapportnummer, ISRN	Klassificering
Totalförsvarets Forskningsinstitut-FOI Avdelningen för Flygteknik, FFA SE-172 90 STOCKHOLM	FOI-R--0243--SE	Vetenskaplig rapport
	Månad År november 2001	Projektnummer C840234
	Verksamhetsgren 3. Flygteknisk forskning	
	Forskningsområde 7. Bemannade och obemannade farkoster	
	Delområde 73. Flygteknisk forskning	
Författare Åsa Hetyei Gunilla Efraimsson	Projektledare Gunilla Efraimsson	
	Godkänd av Torsten Berglind Chef, Beräkningsaerodynamik	
	Tekniskt och/eller vetenskapligt ansvarig Gunilla Efraimsson Beräkningsaerodynamik	
Rapporttitel En numerisk studie av akustiska vågor i ett icke-homogent flöde		

Sammanfattning

En numerisk studie av akustiska vågor som fortplantar sig i ett icke homogent flöde utfördes på en tvådimensionell domän. Ett subsoniskt jetflöde användes som basflöde till vilken en akustisk våg adderades. Det verifierades teoretiskt och numeriskt att den använda jetflödesmodellen upfyllde Euler ekvationerna. I den numeriska verifieringen uppstod instabiliteter i tryck- och hastigetsfälten. Då instabiliteterna reflekterades vid utflödes randen och därmed skulle förstöra de akustiska beräkningarna, gjordes försök att reducera magnituden av instabiliteterna innan de nådde utflödes randen. En undersökning av hur många grid punkter som krävs för att fortplanta akustika vågen i ett icke homogent medium genomfördes.

Nyckelord
Aeroakustik, jet flöde, icke-reflekterande randvillkor,
Övriga bibliografiska uppgifter Examensarbete

ISSN	Sidor	Språk
ISSN 1650-1942	46	Engelska
Distribution enligt missiv	Pris Enligt prislista	
	Sekretess Öppet	